Virology 535 (2019) 111–121

Contents lists available at ScienceDirect

Virology

journal homepage: www.elsevier.com/locate/virology

Efficient RNA silencing suppression activity of *Potato Mop-Top Virus* 8K protein is driven by variability and positive selection

Pruthvi B. Kalyandurg[a,1], Aminallah Tahmasebi[a,b,1], Ramesh R. Vetukuri[c], Sandeep K. Kushwaha[d], Alexander A. Lezzhov[e], Andrey G. Solovyev[f,g], Laura J. Grenville-Briggs[c], Eugene I. Savenkov[a,*]

[a] Department of Plant Biology, Uppsala BioCenter, Swedish University of Agricultural Sciences, Linnean Center for Plant Biology, Uppsala, Sweden
[b] Plant Virology Research Centre, College of Agriculture, Shiraz University, Iran
[c] Department of Plant Protection Biology, Swedish University of Agricultural Sciences, Alnarp, Sweden
[d] Department of Plant Breeding, Swedish University of Agricultural Sciences, Alnarp, Sweden
[e] Faculty of Bioengineering and Bioinformatics, Moscow State University, Moscow, Russia
[f] Belozersky Institute of Physico-Chemical Biology, Moscow State University, Moscow, Russia
[g] Department of Virology Biological Faculty, Moscow State University, Moscow, Russia

ARTICLE INFO

Keywords:
Natural variation
Next generation sequencing
Plant viruses
RNA silencing
siRNA
Viral suppressor of RNA silencing

ABSTRACT

Previously, we investigated the evolution of Potato mop-top virus (PMTV) ORFs. Results indicate that positive selection acts exclusively on an ORF encoding the 8K protein, a weak viral suppressor of RNA silencing (VSR). However, how the extraordinary variability contributes to 8K-mediated RNA silencing suppression remains unknown. Here, we characterized the RNA silencing suppression activity of the 8K protein from seven diverse isolates. We show that 8K encoded by isolate P1 exhibits stronger RNA silencing suppression activity than the 8K protein from six other isolates. Mutational analyses revealed that Ser-50 is critical for these differences. By comparing small RNA profiles we found a lower abundance of siRNAs with U residue at the 5′-terminus after expression of the P1 8K compared to expression of 8K from isolate P125, an isolate with weak VSR activity. These results provide new clues as to the role of positive selection in shaping activities of VSRs.

1. Introduction

RNA silencing, a natural antiviral defence mechanism in plants, also plays vital role in plant development and maintenance of genome stability through *e.g.* suppression of transposons and other foreign nucleic acids, including transgenes. The multiple pathways of RNA silencing target various forms of double-stranded RNA – long perfect duplexes or hairpin-like secondary structures formed by fold-back self-complementarity – for cleavage into small RNAs (sRNAs). These sRNAs typically range from 20 to 24 nucleotides (nt) in size. RNA viruses are potent inducers of RNA silencing. Virus infections are associated with an accumulation of small interfering RNAs (siRNAs) processed from viral dsRNAs, which are formed during virus replication and from extensive secondary structures of viral RNA (Hamilton and Baulcombe, 1999). In plants, DICER-LIKE (DCL) proteins from the RNaseIII family of enzymes mediate the processing of dsRNAs into sRNA duplexes (Csorba et al., 2015; Hiraguri et al., 2005; Hamilton and Baulcombe, 1999). These sRNAs are loaded into Argonaute (AGO) containing RNA-induced silencing complex (RISC), in which one of the sRNA strands serves as a guide to recognise complementary target RNA sequences and to mediate their endonucleolytic cleavage and/or translational repression (Fagard et al., 2000).

In the model plant *Arabidopsis thaliana*, four DCLs are devoted to specialised functions, among which DCL4, DCL2 and DCL3 are involved in antiviral defence by catalysing the production of 21-, 22- and 24-nt virus-derived siRNAs (vsiRNAs), respectively (Margis et al., 2006). In the cytoplasmic pathway of RNA silencing, DCL4 together with dsRNA binding protein 4 (DRB4) produce 21-nt siRNA duplexes (Fukudome et al., 2011), whereas DCL2 catalyses production of 22-nt siRNAs acting redundantly or in cooperation with the products of DCL4 (Parent et al., 2015). Together DCL4 and DCL2 confer efficient antiviral defence and the products of their catalytic activity, namely, 21- and 22-nt viral siRNAs, are usually the most abundant classes of siRNAs in virus-infected plants (Deleris et al., 2006). Most higher plants encode at least

* Corresponding author.
E-mail address: eugene.savenkov@slu.se (E.I. Savenkov).
[1] These authors contributed equally to this work.

https://doi.org/10.1016/j.virol.2019.06.018
Received 18 April 2019; Received in revised form 27 June 2019; Accepted 29 June 2019
Available online 01 July 2019
0042-6822/

10 *AGO* genes and their isoforms, although the precise contribution of AGOs to antiviral silencing remains largely unknown for most plant species (Odokonyero et al., 2017). In *Arabidopsis*, antiviral silencing requires the cooperative action of AGO1 and AGO2, whereas AGO5, AGO7 and AGO10 can also contribute to the defence (Qu et al., 2008; Wang et al., 2011; Zhang et al., 2012; Garcia-Ruiz et al., 2015). Sorting of virus-derived siRNA into AGO-containing multiprotein complexes is directed by the 5′-terminal nucleotide residue (Mi et al., 2008).

Viral suppressors of RNA silencing (VSRs) counteract different steps in the RNA silencing pathway and employ various strategies to suppress antiviral RNA silencing, including binding of dsRNA (Sahana et al., 2014; Qu et al., 2003; Chen et al., 2008) and, thus, competing for its cleavage, inhibiting the functioning of DCL proteins (Qu et al., 2003; Lacombe et al., 2010), inactivating DRB (Laird et al., 2013; Haas et al., 2008), interacting with and inducing degradation of AGO proteins (Jin and Zhu, 2010; Varallyay and Havelda, 2013), inhibiting RDR functioning (Zhang et al., 2008; Okano et al., 2014; Li et al., 2014), and sequestering vsiRNA (Silhavy et al., 2002; Molnar et al., 2010) thereby helping the virus in its efficient multiplication, movement and efficient accumulation in the host (Csorba et al., 2015). An emerging common theme from the current studies is that single VSRs can target more than one step in antiviral RNA silencing pathways, thus, supporting the concept of the multifunctionality of viral proteins (Valli et al., 2018; Iki et al., 2017).

Host defence and viral counter-defence result in selection pressure on both actors; this phenomenon is often referred to as evolutionary ‘arms-race’, *i.e.* antagonistic coevolution. Therefore, it is expected that the evolution of VSRs should be of paramount importance for a successful viral infection of their hosts. Indeed, recently, in a study on the diversity of potato mop-top virus (PMTV), we reported that the open reading frame (ORF) encoding the 8K protein, a weak VSR, is under strong diversifying selection, whereas all other PMTV cistrons are under neutral (purifying) selection (Kalyandurg et al., 2017).

PMTV, the type member of genus *Pomovirus* within the family *Virgaviridae*, is an economically important pathogen that causes ‘potato spraing’ disease characterised by formation of necrotic arcs inside the potato tuber flesh making the tubers unmarketable (Adams et al., 2009; Calvert and Harrison, 1966). The tripartite positive-sense single-stranded RNA genome of the virus encodes six open reading frames (ORFs) (Scott et al., 1994; Kashiwazaki et al., 1995). The genomic segment RNA-rep encodes proteins involved in the replication of the virus (Savenkov et al., 1999). The proteins encoded by the second segment, RNA-CP, are needed for virus encapsidation (Kashiwazaki et al., 1995) and transmission by the soil-inhabiting vector *Spongospora subterranea* (Reavy et al., 1998). The third segment, RNA-TGB, codes for a triple gene block (TGB) module of movement proteins (Scott et al., 1994) and a small 8 kDa protein (8K), a week VSR (Lukhovitskaya et al., 2005). Although, dispensable for the long-distance movement of the virus in *Nicotiana benthamiana* and in *N. tabacum*, the 8K protein appears to be important for efficient virus accumulation in these hosts (Lukhovitskaya et al., 2013). 8K is structurally classified as a zinc-finger protein with a putative SWIM zinc-finger motif characterised by a consensus sequence $CxCx_nCxC$, where C refers to cysteine residues and x refers to any amino acid residue (Kalyandurg et al., 2017).

Recently, we defined four major 8K clades based on comparison of the sequences from more than 80 PMTV isolates (Kalyandurg et al., 2017). In general, the variability of the 8K protein sequences is significantly higher among Peruvian isolates of PMTV as compared to the sequences from the rest of the world (Kalyandurg et al., 2017). Hence, we hypothesized that these might be due to greater diversification of the 8K sequences through positive selection as a result of PMTV adaptation to more than 5000 potato varieties and potato sub-species found in Andean region of Peru, the centre of potato domestication (International Potato Center, 2017). However, the importance of this high diversity for the functioning of the 8K protein has not been addressed so far.

Here, we have analysed RNA silencing suppression activity of the 8K protein from seven diverse PMTV isolates (referred to as *8K* alleles) representing four 8K clades (Kalyandurg et al., 2017). While expression of 6 alleles led to weak suppression of RNA silencing, the suppression effect was much stronger, but still moderate relative to potyviral HcPro, upon expression of the *P1* allele. Through site-directed mutagenesis we identified Ser-50 as being important for enhanced RNA silencing suppression activity of $8K^{P1}$ compared to very weak suppression by $8K^{P125}$. We thus conducted further experiments on 8K using two contrasting natural variants of the protein showing moderate ($8K^{P1}$) and very weak ($8K^{P125}$) silencing suppression activities. Analysis of normalised siRNA abundance through Next Generation Sequencing (NGS) of small RNA species revealed lower accumulation of certain classes of siRNAs upon expression of the *P1* allele relative to expression of the *P125* allele. Our results suggest that 8K might affect several steps in the RNA silencing pathway, and pave the way for follow-up studies on mechanisms of silencing suppression by 8K. It is likely that other weak VSR could be under positive selection, and some of their natural variants could be more potent in suppression of RNA silencing than the others.

2. Results

2.1. Comparison of VSR activity of seven natural variants of PMTV 8K

To compare the anti-silencing properties of natural variants of the 8K protein, we quantified the number of cells within fluorescent loci (as well as a total area of infection) formed by complementation of cell-to-cell movement of a sGFP-expressing turnip crinkle virus (TCV-sGFP) as the reporter of silencing suppression activity of co-expressed *8K* alleles (Table 1). The cell-to-cell movement of TCV-sGFP is compromised due to host antiviral silencing, because the TCV genome was modified to express sGFP instead of the native coat protein (CP), a strong VSR (Powers et al., 2008; Qu et al., 2003). Thus, TCV-sGFP is usually confined to single cells, but gains the ability to move to neighbouring cells if a VSR is provided *in trans*. In this assay, the 35S:HcPro construct as well as constructs designed to express myc-tagged natural variants of the 8K protein were delivered into *N. benthamiana* leaves via agroinfiltration followed by inoculation with TCV-sGFP transcripts. To this end, seven most diverse alleles, representing four major clades of the 8K sequences identified so far, were selected (Fig. 1; Table 1) and placed downstream of the 35S promoter in the binary vector pGWB18 (Nakagawa et al., 2007). Potato virus A (PVA) HcPro (pGWB18-HcPro) and the empty plasmid (EP) pGWB were used as positive and negative controls, respectively. The infiltrated patches of *N. benthamiana* leaves were rub-inoculated with in vitro generated TCV-sGFP transcripts one day post infiltration (dpi). Four days post inoculation the levels of silencing suppression were assayed by monitoring the fl33uorescent foci formed by TCV-sGFP movement (Table S1), measuring the area of TCV-sGFP infection and by measuring the intensity of fluorescence (Fig. 2A and B). The mean area of infection in leaf patches infiltrated for expression of *P1* allele was larger (mean value of 5.5×10^4 μm^2) than

Table 1
8K alleles used in the study and efficiency of RNA silencing suppression activity associated with their expression.

8K allele	Origin	VSR efficiency
P1	natural, Peru	*****
P11	natural, Peru	**
P13	natural, Peru	**
P118	natural, Peru	***
P125	natural, Peru	**
P157	natural, Peru	***
SwH	natural, Sweden	***
C18G	mutant of *P125*	**
N50S	mutant of *P125*	*****
C34A C36A	mutant of *SwH*	–

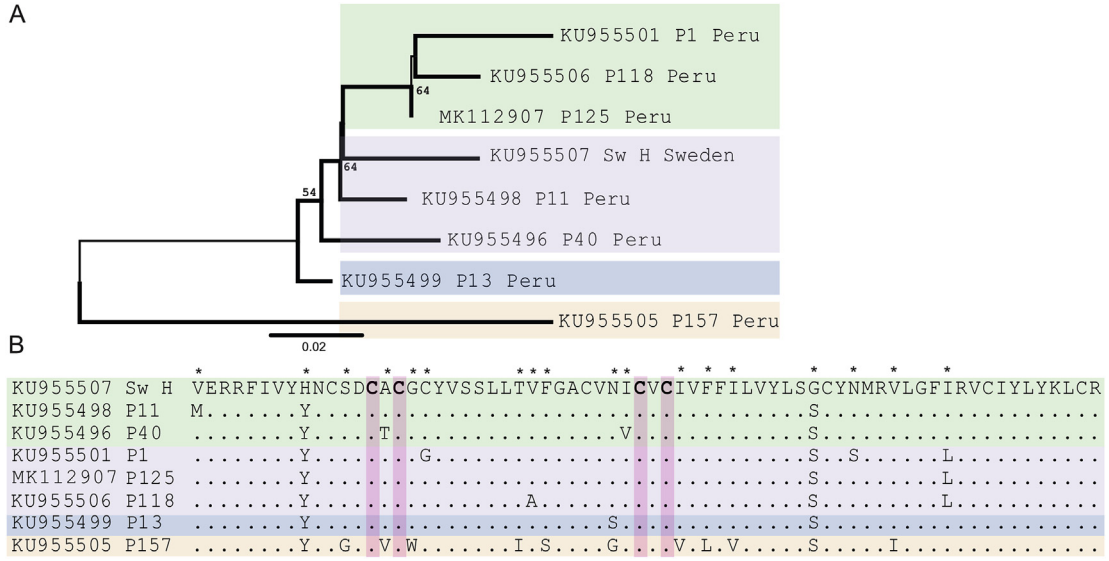

Fig. 1. Phylogenetic relationship and sequence variability among sequences of the 8K protein used in this study. (A) The neighbour-joining (NJ) tree of 8K amino acid sequences representing four different clades. (B) Multiple sequence alignment showing amino acid differences in the sequences of the 8K protein. Variable positions are indicated with an asterisk. Cysteine residues involved in the formation of a putative SWIM zinc-finger motif are highlighted.

those of six other alleles (measuring from ~2.1x10^4 to 3.6 × 10^4 μm^2), but still lower than the area of infection formed by complementation with PVA HcPro (mean value of 9.7 × 10^4 μm^2), indicating that 8K^{P1} is relatively moderate in suppression of silencing as compared to PVA HcPro, but stronger than six other natural 8K variants.

To exclude the possibility that the relatively weak silencing suppression activity of 8K^{SwH}, 8K^{P11}, 8K^{P13}, 8K^{P118}, 8K^{P125} and 8K^{P157} is due to low levels of expression of the respective proteins in infiltrated leaf patches, the levels of protein accumulation were examined by immunoblotting with a monoclonal antibody specific to the myc epitope. Notably, 8K^{SwH}, 8K^{P11}, 8K^{P13}, 8K^{P118}, 8K^{P125} and 8K^{P157} accumulated at levels slightly higher than that of 8K^{P1} (Fig. 2D) indicating that relatively higher silencing suppression activity of 8K^{P1} is not due to higher levels of protein expression.

Our earlier attempts, before the advent of TCV-sGFP complementation assay, to demonstrate anti-silencing activity of 8K^{SwH} (the 8K protein encoded by a Swedish isolate of PMTV) in a standard transient silencing suppression assay did not reveal such a function (Lukhovitskaya et al., 2005). However, identification of 8K^{P1} as a moderate VSR compared to the 8K protein encoded by six other isolates prompted us to analyse 8K^{P1} (as well as 8K$^{Sw\ H}$, 8K^{P11}, 8K^{P13}, 8K^{P118}, 8K^{P125} and 8K^{P157}) in a conventional transient silencing suppression assay, in which the GFP mRNA, expressed by agroinfiltration of wild type (wt) *N. benthamiana* leaves, serves both as an inducer and as a target of RDR6-dependent sense-mediated post-transcriptional gene silencing (PTGS). Co-expression of a VSR prevents GFP silencing from occurring and results in greater GFP fluorescence under UV light and higher GFP accumulation as compared to an empty plasmid (EP) control. To examine the efficiency of seven natural variants of the 8K protein in suppressing sense-mediated RNA silencing, agrobacteria with the 35S:GFP construct was co-infiltrated with agrobacteria cultures for expression of seven *8K* alleles (pGWB18-8K^{P1}, -8K$^{Sw\ H}$, – 8K^{P11}, -8K^{P13}, -8K^{P118}, -8K^{P125} and -8K^{P157}constructs, respectively). PVA HcPro (pGWB18-HcPro) and EP were used as positive and negative controls, respectively. The infiltrated patches of wt *N. benthamiana* leaves showed green fluorescence under UV illumination 2 dpi in all the samples tested (Fig. S1A). However, at 5 dpi, the GFP fluorescence was almost completely lost in all treatments except for HcPro and 8K^{P1} (Fig. 2E and Fig. S1A). These data suggest 8K from the P1 isolate, but not from six other isolates tested, is able to suppress onset of sense-mediated PTGS, albeit not as strongly as HcPro. The visual observations were confirmed by quantification of accumulation of the GFP protein and the GFP transcript by immunoblotting and qRT-PCR, respectively (Fig. 2F and Fig. S1B). The levels of GFP protein and *GFP* mRNA were higher in the presence of 8K^{P1} compared to other treatments, although not as high as in the presence of HcPro (Fig. 2F, Fig. S1B and data not shown).

2.2. A single amino acid difference in 8K contributes to enhanced suppression of RNA silencing

Having identified 8K^{P1} as being a moderate VSR, it did not escape our attention that 8K^{P1} differs from 8K^{P125}, a weak VSR, by two amino acid residues, namely ^{P1}G18C^{P125} and ^{P1}S50N^{P125}. We thus tested the effects of these amino acid residues on silencing suppression activity of the 8K protein. To individually identify which of these two amino acid residues contribute to higher levels of RNA silencing suppressing activity, we carried out site-directed mutagenesis to generate two P125 mutant alleles: *C18G* and *N50S* (Fig. 3A; Table 1). Upon introduction of the cognate point mutations, the *P125* allele as well as *P1* allele were expressed in *N. benthamiana* leaves by agroinfiltration and the effects of the corresponding proteins (8K^{C18G}, 8K^{N50S}, 8K^{P125} and 8K^{P1}) on suppression of RNA silencing was tested in TCV-sGFP complementation assay (Fig. 3B). As before, expression of the *P1* allele led to efficient complementation of TCV-sGFP movement, resulting in larger infection foci (mean area of 4.7 × 10^4 μm^2; Fig. 3B and C). On the other hand, expression of *P125* and its mutant allele *C18G* (Fig. 3D) resulted in TCV-sGFP infections confined into a smaller area of infection, with mean value of ~2.3 × 10^4 μm^2 in area (Fig. 3B and C). Expression of the *N50S* mutant allele of *P125* (Fig. 3D) led to the formation of larger TCV-sGFP foci (mean area of 4 × 10^4 μm^2; Fig. 3B and C). Taken together, these results indicate the importance of Ser-50 for efficient 8K-mediated suppression of RNA silencing.

2.3. Disruption of a putative SWIM zinc finger motif eliminates the RNA silencing suppression activity of 8K

To examine the effect of cysteine residues of a putative SWIM zinc finger motif on silencing suppression capacity of the 8K protein we performed site-directed mutagenesis. We engineered a *SwH* mutant allele, *C34A C36A*, by replacing conserved cysteines of the zinc finger motif with alanine residues (Table 1; Fig. 4A). We then tested the effect

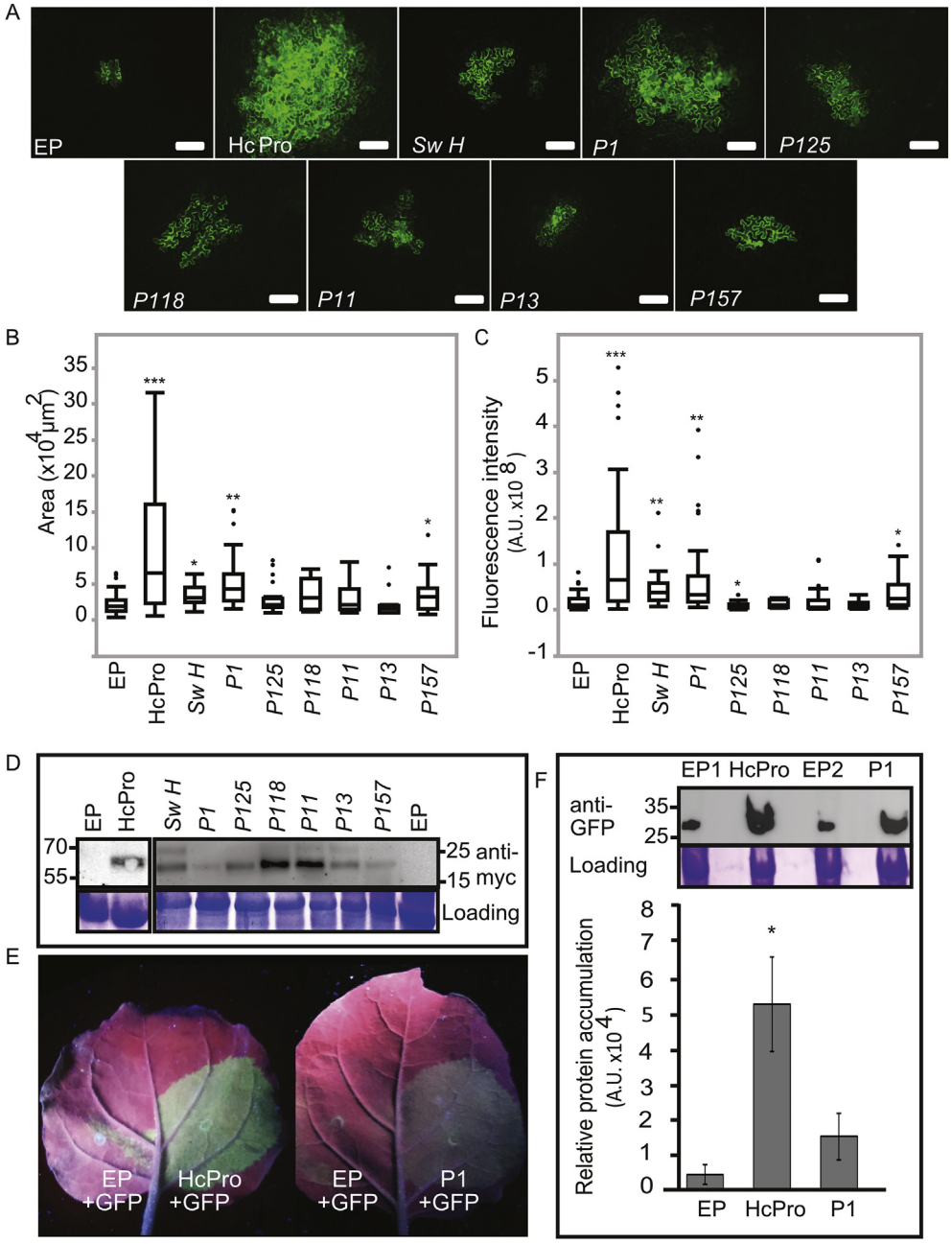

Fig. 2. Silencing suppression activity of natural variants of the 8K protein. (A) Representative fluorescence microscopy images showing the movement of TCV-sGFP to neighbouring cells in the presence of HcPro, and upon expression of the *8K* alleles as indicated in the panels. EP, empty plasmid control. Bar, 100 µm. (B) Box plot showing the area of TCV-sGFP infection for each VSR tested. (C) Mean fluorescence intensity of the same TCV-sGFP infection foci shown in (B). (B and C) Box plot represents 25th to 75th percentile and whiskers extend to 1.5 X interquartile region from the box. The horizontal bar in each box represents the median value. Black dots above each box indicate outliers. Asterisks indicate statistically significant difference relative to empty plasmid control; ***P < 0.0001; **P < 0.005; *P < 0.05, Dunnett's test. A.U., arbitrary units (D) Immunoblotting with anti-myc antibodies showing expression of HcPro and natural variants of the 8K protein (top panel). Coomassie staining shows the loading of the samples (lower panel). (E) *Nicotiana benthamiana* leaves 4 days post agroinfiltration with GFP construct co-infiltrated either with EP control, or constructs expressing HcPro or *P1* allele of *8K*. (F) Quantification of GFP accumulation using immunoblot analysis with anti-GFP antibodies.

of expression of this mutant allele on suppression of RNA silencing in TCV-sGFP assay. Upon agroinfiltration for expression of $8K^{SwH}$ as well as its derivative $8K^{C34A\ C36A}$ followed by inoculation with TCV-sGFP transcripts, as expected, $8K^{SwH}$ complemented the virus movement to neighbouring cells forming foci consisting of up to 18 cells 4 days post inoculation. However, in the presence of $8K^{C34A\ C36A}$ or EP the virus infection was mostly limited to one to three cells (Fig. 4B; Table S1). Consistently, the area of the TCV-sGFP infection was significantly smaller in size when co-expressing the *C34A C36A* mutant allele as compared to the wt allele (Fig. 4C), indicating that integrity of the putative SWIM zinc finger motif is essential for the 8K protein to act as a VSR. The accumulation of $8K^{SwH}$ and $8K^{C34A\ C36A}$ in the infiltrated patches was confirmed by immunoblotting and appeared to be at similar levels (Fig. 4D).

2.4. Deep sequencing of sRNA reveals lower accumulation of certain small RNAs in the presence of $8K^{P1}$

Although $8K^{P1}$ is able to suppress sense transgene-induced silencing in an agroinfiltration assay, until now, however, there has been no analysis of sRNA in the presence of $8K^{P1}$. Moreover, comparison of sRNA profiles between weak (i.e. $8K^{P125}$), moderate (i.e. $8K^{P1}$) and strong (i.e. HcPro) VSRs could provide insights into the mechanisms of RNA silencing suppression. To investigate this possibility, we sequenced sRNAs resulting from the sense mediated PTGS.

To characterize the distribution and abundance of sRNA species in the presence the VSRs, 12 sRNA libraries were constructed using total RNAs isolated from *N. benthamiana* leaves agroinfiltrated for expression of *GFP* gene along with either *P1* or *P125* alleles or PVA *HcPro* as a positive control or EP as a negative control, respectively. The samples were collected 4 dpi and included three biological replicates for each treatment. Each biological replicate represented a pool of leaves from

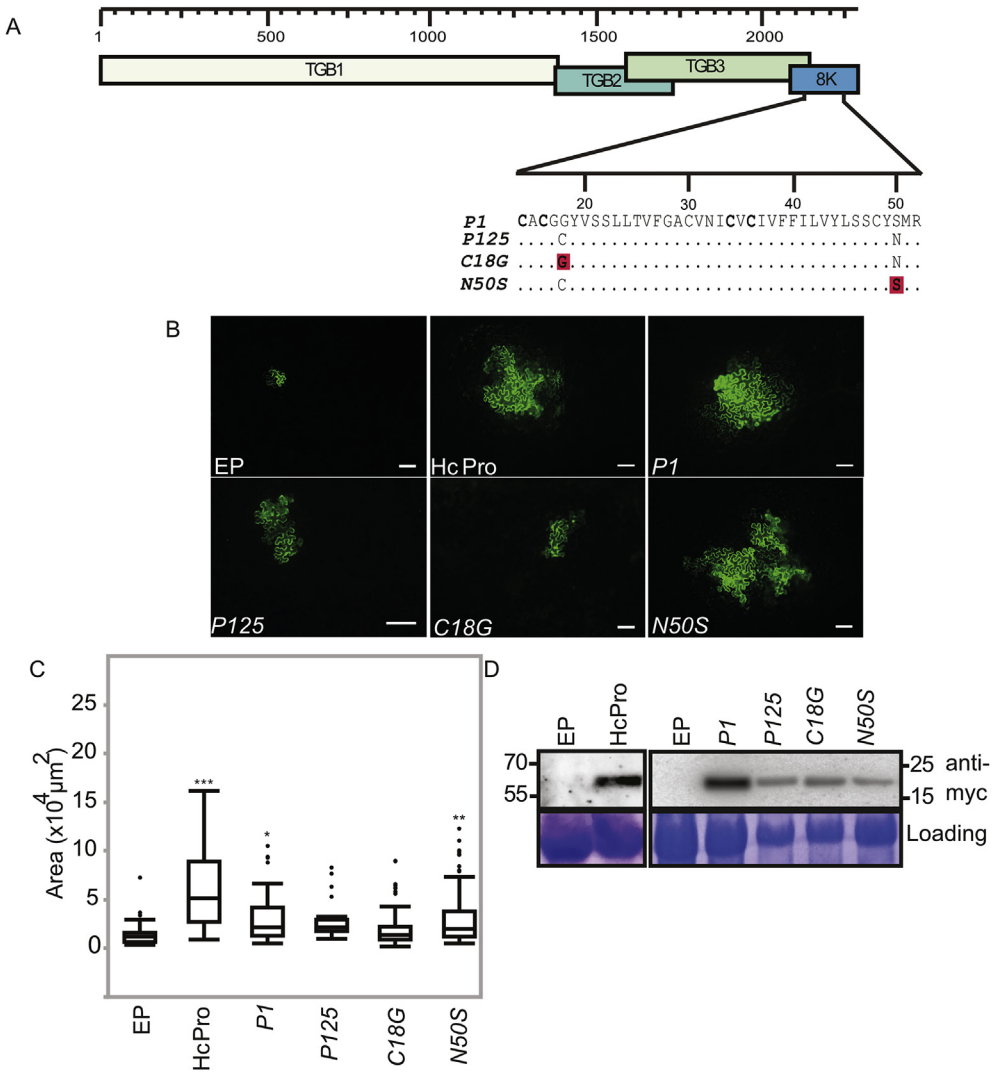

Fig. 3. Ser-50 influences RNA silencing suppression activity of the 8K protein. (A) Schematic representation of the ORF for triple gene block (TGB) and the 8K protein and 8K derivatives generated by site specific mutagenesis of the *P125* allele. Mutagenesis was carried out to replace Cys-18 with Gly (C18G), and Asn-50 with Ser (N50S) individually (highlighted in red). (B) Representative images of fluorescence microscopy showing an increase in cell-to-cell movement of TCV-sGFP in *N. benthamiana* leaves infiltrated for expression of the *N50S* allele as compared to those of *P125* and *C18G*. Bar, 100 µm. (C) Quantification of the area of infection foci. Box plot represents 25th to 75th percentile and whiskers extend to 1.5 X interquartile region from the box. The horizontal bar in each box represents the median value. Black dots above each box indicate outliers. Asterisks indicate statistically significant difference relative to empty plasmid control; ***P < 0.0001; **P < 0.005; *P < 0.05, Dunnett's test. (D) Immunoblotting showing expression of HcPro and the 8K protein from its various alleles used in these experiments.

three individual plants. The sequencing was performed with an Illumina HiSeq2500 instrument and each biological replicate generated ~12.4 million to 33.7 million clean reads ranging from 18 to 30 nt (Table S2; Fig. S2). For each treatment, three biological replicates were analysed individually and showed very similar patterns (Fig. S2).

The results described below represent the averages obtained from three biological replicates. Total reads obtained from the sequencing were aligned to the sGFP transgene sequence using Bowtie v-1.2.2 with 2 mismatches allowed in the seed region and no mismatches in the read alignment (v 0). 1.35 to 3.83 million sRNA reads matching *GFP* were identified accounting for 3.8–11.1% of the total reads (Fig. 5A, Table S2). The normalized size distribution of total sRNAs within each treatment was dominated by 21-nt species (30–48%), followed by 22-nt and 24-nt sRNA populations, representing 22–34% and 11–32% percent respectively (Fig. 5B). Further analyses were performed by aligning canonical sRNAs of the 21-nt, 22-nt and 24-nt size classes to the GFP transgene sequence (Fig. 5C). The single-nucleotide resolution maps generated for each treatment, namely, EP, HcPro, *P1* and *P125*, indicated that siRNAs of sense and antisense polarities were almost continuously scattered throughout the *GFP* ORF (Fig. 5C) with almost similar amounts of sense and antisense siRNAs suggesting that siRNAs were derived from both sense and antisense GFP RNA transcript strands to a similar extent (Fig. 5C). Moreover, the total number of GFP siRNAs varied in each treatment with higher number of GFP siRNAs being detected in the presence of EP control - 10.9% of the total sRNA reads (Fig. 5A, Table S2). On the other hand, the number of GFP-specific siRNA in the presence of VSRs, namely, $8K^{P125}$, $8K^{P1}$ and HcPro had similar coverage of a total of 4.0%, 5.3%, and 4.5%, respectively, which was lower compared to the EP control (Fig. 5A, Table S2).

To explore the origin of siRNAs, the size and polarity distribution of siRNAs were characterized further. Size distribution analysis showed that siRNAs produced from the GFP transgene were predominantly 21-, 22- and 24-nt in length, suggesting that three canonical DCLs, namely, DCL4, DCL2 and DCL3, might be the predominant Dicer-like RNasesIII involved in siRNAs biogenesis (Fig. 5B). Polarity distribution analysis revealed almost equivalent amounts of sense and antisense strands of siRNAs (Fig. 5C and D), although the differences in amount of sense- and antisense strands were obvious in 21-, 22- and 24-nt siRNAs only when the HcPro treatment was compared with other treatments.

The observed differences in the accumulation of siRNAs prompted us to validate the NGS data by RT-qPCR. To this end, using sRNA data sets, we randomly selected six abundant siRNAs scatted along GFP ORF sequence (Fig. 6A, Table S3) and employed a quantitative stem-loop RT-PCR method (Fig. 6B) for detection of the antisense strand of these sRNAs (Varkonyi-Gasic and Hellens, 2011). The sRNAs selected for validation by RT-qPCR represented two major size classes (21- and 22-nt) of siRNA involved in anti-viral defence (Fig. 6A). To investigate the abundance change in accumulation of these siRNAs, RT-qPCRs were conducted using total RNAs isolated 5 dpi from *N. benthamiana* leaves infiltrated for expression of *GFP* along with either *HcPro*, or the *P1*

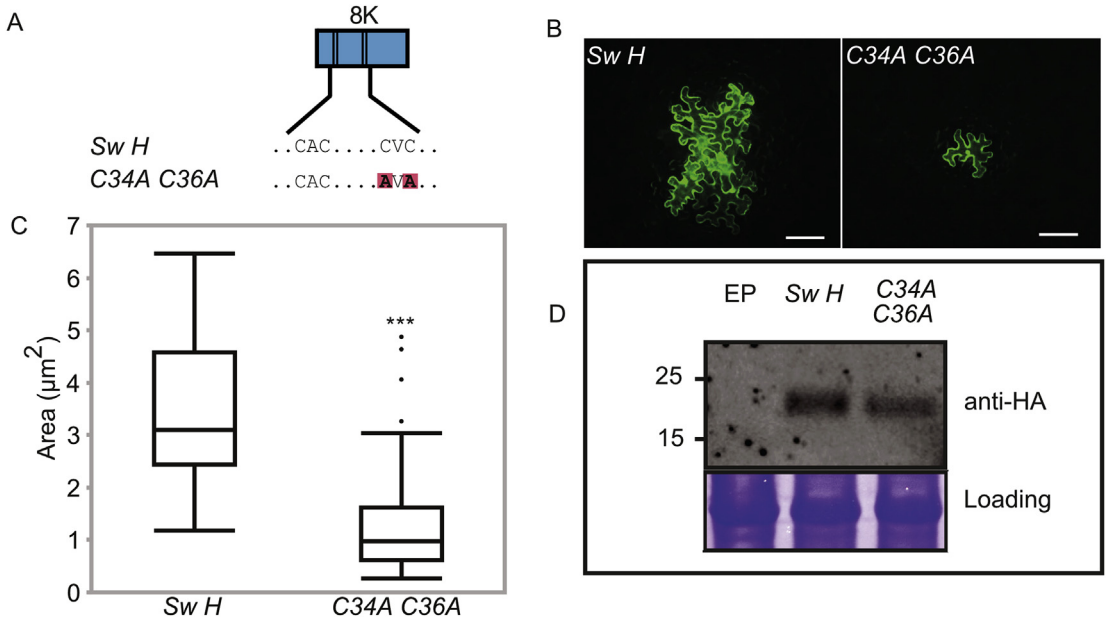

Fig. 4. Integrity of a putative SWIM zinc-finger motif is indispensable for RNA silencing suppression activity of the 8K protein. (A) Schematic representation of the 8K protein. Black vertical lines represent Cys residues. Ala residues replacing Cys residues as a result of mutagenesis are highlighted in red. (B) Fluorescence microscopy images showing impaired cell-to-cell movement of TCV-sGFP in complementation assay upon expression of the *SwH* mutant allele C34A C36A. Bar, 100 μm. Images were taken 4 days post inoculation with TCV-sGFP. (C) Quantification of the area of the infection foci. Box plot represents 25th to 75th percentile and whiskers extend to 1.5 X interquartile region from the box. The horizontal bar in each box represents the median value. Black dots above each box indicate outliers. Asterisks indicate significant statistical difference relative to *Sw H*; ***$P < 0.0001$, Dunnett's test. (D) Immunoblotting for detection of HA-tagged $8K^{SwH}$ protein (expression of *Sw H* allele), and $8K^{C34A\ C36A}$ (expression of C34A C36A allele). Coomassie staining shows the loading of the samples (lower panel).

allele, or the *P125* allele, or the EP negative control. Additionally, we analysed expression of miR166, which is highly expressed in leaves (Baksa et al., 2015). There were no significant changes (Student's two-tailed *t*-test, $P > 0.05$) in the accumulation levels of the 21-nt siRNAs (Fig. 6C), whereas, for most of the samples, the levels of 22-nt siRNAs were significantly lower (Student's two-tailed *t*-test, $P < 0.05$) in the presence of the VSRs relative to EP control (Fig. 6C) with no significant differences between *HCPro*, *P1* and *P125* treatments. The pattern of miR166 expression differed from that of GFP-specific siRNA and showed slight, but statistically significant (Student's two-tailed *t*-test, $P < 0.05$) increase in the presence of HcPro and $8K^{P1}$. A regression analysis (Fig. S3) showed a weak positive correlation (Pearson's correlation coefficient, r = 0.358) between number of reads corresponding to siRNAs in the NGS data and quantification of siRNAs by RT-qPCR (Fig. S3).

Selective loading of sRNAs into specific AGOs is preferentially directed by the 5′-terminal nucleotide (Mi et al., 2008). To find out whether sRNAs are potentially sorted into distinct AGO complexes, the relative abundance of sRNAs according to the nucleotide residue at their 5′-terminus was analysed. For the EP control samples, U was the most abundant nucleotide residue at the 5′-end of 21-, and 22-nt siRNA size classes (38 and 39%, respectively; Fig. 5E). These data suggest that in the EP control samples, where RNA silencing is active and ongoing, 21-, and 22-nt sRNAs are preferentially loaded into AGO1, which shows preference for U. A similar pattern of the ratio and of the terminal nucleotide preference was observed in the presence of a weak VSR, $8K^{P125}$ (Fig. 5E). In contrast, in the presence of $8K^{P1}$ or HC-Pro the ratio of the four nucleotide residues showed statistically significant difference (Student's one-tailed *t*-test, $P < 0.05$; Fig. S4) as compared to the EP ratio – with an obvious decrease in abundance of U at the 5′-end – ranging from 23 to 31% depending on size class. Collectively, the data suggest that $8K^{P1}$ (as well as HcPro) might interfere with stability of siRNAs sorted into AGO1-contaning complexes.

3. Discussion

Viruses and their host are entrenched in an evolutionary arms race (antagonistic coevolution). Hosts evolve mechanisms to suppress virus multiplication and virulence, whereas viruses, which highjack host machinery for replication and survival, develop counteracting strategies to escape host defences. Both processes contribute to strong selection for viral adaptation. This is especially true for RNA viruses, which, compared to DNA viruses, are relatively well understood in an evolutionary context. In general, due to low-fidelity of their RNA polymerases required for replication, RNA viruses have high mutation rate, which provides ample material for adaptive evolution (Coffey et al., 2011; Pfeiffer and Kirkegaard, 2005).

Previously, we looked for signatures of selection between complete genomic segments of PMTV isolates infecting potato in Peru and other parts of the world. We found that most of PMTV genome is under purifying (neutral) selection, with only one gene evolving adaptively, suggesting that this particular gene might be a key in antagonistic evolution to escape suppression by the host defence machinery. Intriguingly, this gene is appeared to encode a VSR (PMTV 8K protein), indicating that adaptive evolution of PMTV is directly linked to suppression of RNA silencing, the host anti-viral defence mechanism. A hallmark of adaptive evolution across a phylogeny is evidence of multiple nucleotide residue substitutions at the same codon. Indeed, we identified significantly positively selected amino acid residue substitutions throughout *8K* sequence with *dN/dS* values of > 1 (Kalyandurg et al., 2017). Moreover, comparison of eighty six 8K sequences available so far revealed 23 variable sites per 68-amino-acid-residues-long protein – an extraordinary variability considering the size of the protein, literally, with every third amino acid residue being variable.

Positive selection acting on VSRs ensures high diversity of their alleles, which can be advantageous in selecting those alleles, which provide better suppression of anti-viral RNA silencing, *e.g.* by counteracting more than one step of the RNA silencing pathway (Iki et al., 2017). Indeed, some plant VSRs are reported to display a great

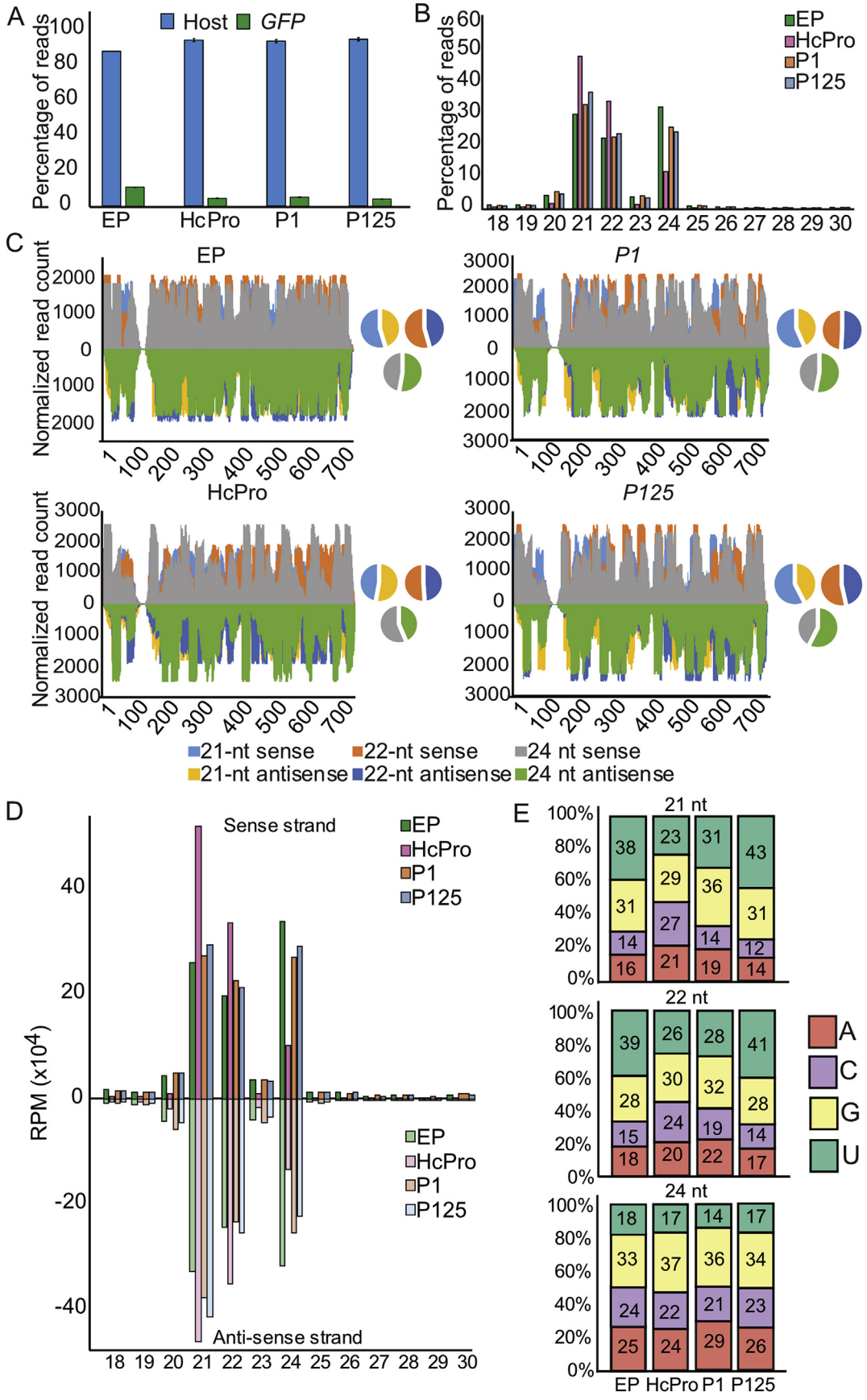

(caption on next page)

Fig. 5. Profile of 21-24-nucleotide (nt) *GFP*-derived small interfering RNAs (siRNAs) from GFP-agroinfiltrated wt *Nicotiana benthamiana* plants co-expressing EP, HcPro as well as P1 and *P125* alleles of *8K*. (A) Percentage of total sRNA reads (18–30 nt) mapped to the host (*N. benthamiana*) versus sRNA reads mapped to the *GFP* gene. (B) Size distribution of 18–30 nt small RNAs mapped to the *GFP* gene. (C) Single-nucleotide resolution maps of *GFP*-derived siRNAs aligned to the *GFP* gene of both positive and negative polarity (indicated with different colours). The pie charts to the right of each graph show percentage of sense to antisense siRNA accumulation in each treatment. Cumulative data from all three biological replicates are shown. (D) Strand polarity of 18–30 nt GFP derived siRNAs. The graphs show read-count per million mapped reads. (E) Relative abundance of each of four nucleotides at the 5′-terminus of 21-, 22-, and 24- nt *GFP*-derived siRNAs. The data represent averages of three biological replicates.

sequence variability (Murray et al., 2013). However, it is of particular interest to evaluate how these variable VSRs perform when encountered with the host's own defences, namely, RNA silencing. Therefore, we sought to compare the VSR activity of the natural variants of 8K from the Andean region of Peru, the centre of PMTV diversity (Kalyandurg et al., 2017). To this end, seven the most diverse *8K* alleles, belonging to four clades defined based on a comparison of all 8K sequences available so far (42), were characterized using TCV-sGFP complementation assay. The significant advantages of TCV-sGFP complementation method include the high precision of measurement of infection foci size and/or of the number of the cells within foci. This allows a better comparison of RNA silencing suppression efficiency of the proteins of interest in terms of these quantitative parameters. These advantages enabled us to show a wide range of RNA silencing suppression activities of the 8K protein from various PMTV isolates, *i.e.* compared to a strong VSR, PVA HC-Pro, $8K^{P1}$ displayed a moderate VSR activity, followed by $8K^{SwH}$, $8K^{P118}$ and $8K^{P157}$, which showed significantly weaker VSR activity, whereas $8K^{P11}$, $8K^{P13}$, and $8K^{P125}$ were the weakest among characterised. In a pioneering study on the role of sites under positive selection in modulating an RNA silencing suppressor activity, the authors demonstrated that a VSR encoded by *Rice Yellow Mottle Virus* (RYMV) shows a wide range of diversity in efficiency of RNA silencing suppression depending on the origin of the isolate (Sire et al., 2008). Moreover, these differences correlated with amino acid changes at the sites under positive selection as was demonstrated by site-directed mutagenesis (Sereme et al., 2014). Altogether RYMV data and our data (this study) support the notion that positive selection shapes anti-silencing activities of some VSRs, which appear to evolve in order to adapt to the defence pressure of anti-viral RNA silencing and to ensure efficient virus multiplication, abundant accumulation in a host tissue (for efficient virus transmission) and spread.

Previous studies – on *e.g.* HcPro of potyviruses – have reported that certain point mutations leading to amino acid substitutions in VSRs can affect their RNA silencing suppression function (Gonzalez-Jara et al., 2005; Yambao et al., 2008; Torres-Barcelo et al., 2008; Torres-Barcelo et al., 2010). Intriguingly, a pairwise sequence alignment indicated that $8K^{P1}$and $8K^{P125}$, showing a moderate and very weak RNA silencing suppression activity, respectively, differ only by two amino acid residues at positions 18 and 50. This observation prompted us analyse the individual contribution of these amino acid residues to the efficiency of 8K-mediated RNA silencing suppression. Through mutagenesis we demonstrated that Ser-50 is important for such a function. Considering that serine is one of three amino acid residues that are commonly phosphorylated by kinases in eukaryotic organisms, we cannot exclude the possibility that phosphorylation at Ser50 in $8K^{P1}$, might contribute to the efficiency of RNA silencing suppression by this particular variant of PMTV 8K. Indeed, phosphorylation of serine residues was shown to exert an effect on the functions of some VSRs including γb of *Barley Stripe Mosaic Virus* and the 2b protein of *Cucumber Mosaic Virus* (Zhang et al., 2018; Nemes et al., 2017).

Another aspect uncovered in this study is that all but one *8K* allele isolated from different strains of PMTV were inert in a standard transient silencing suppression assay or weak in the TCV-sGFP assay, despite the conservation of an SWIM zinc-finger motif shown to be essential for the 8K protein functioning as a VSR (this study). Given the lack of the ORF for the 8K protein in other pomoviruses, including two novel recently discovered and characterised pomoviruses of potato (Gil et al., 2016), our interpretation is that silencing suppression capacity of 8K is a recently emerging feature of this particular pomovirus. It seems that the 8K sequence is still evolving towards some further silencing suppression activity as exemplified by the *P1* allele. Alternatively, it is equally possible that most of the *8K* alleles tested in this study in *N. benthamiana* do provide efficient suppression of RNA silencing in the natural host of PMTV – potato, or, at least, in some potato varieties. Considering, that all but one *8K* alleles tested in this study originate from Peru, the centre of potato domestication, where farmers grow more than 5000 potato varieties; it is also possible that some of the *8K* alleles are adapted to certain potato cultivars or other related *Solanum*

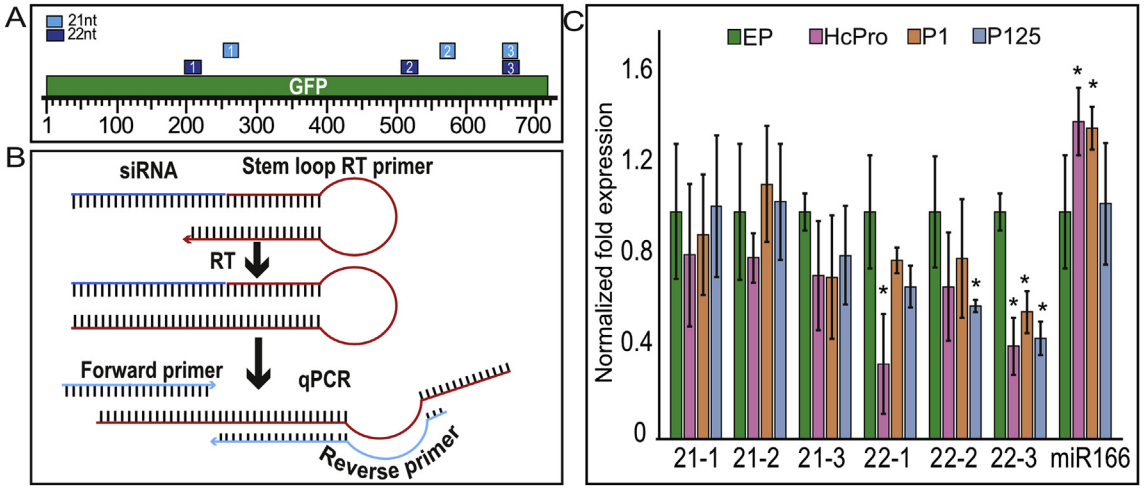

Fig. 6. Quantification of *GFP*-derived 21- and 22-nt siRNAs, and miR166 using quantitative stem-loop RT-PCR. (A) Schematic representation of the positions of 21- and 22-nt siRNAs selected for the quantification. (B) Graphical representation of the stem-loop RT-qPCR principle. Reverse transcription was carried using a stem-loop RT primer that binds to the 3'-end of the siRNA. Then the RT product is used as template for the qPCR with a siRNA-specific forward primer and a universal reverse primer. (C) Relative fold expression of 21- and 22-nt siRNAs and miR166 normalized to the expression of *NbPP2A*. Asterisks indicate significant statistical difference relative to EP control; $*P < 0.05$; Student's two tailed *t*-test.

species indigenous to this area.

Using global sRNA-seq and real-time PCR analysis, we identified some differences in accumulation of certain classes of siRNA in the presence of VSRs analysed in this study. These differences included: (i) reduction in accumulation of the antisense strand of 22-nt siRNAs in the presence of three VSRs, HC-Pro, $8K^{P1}$ and $8K^{P125}$; (ii) lower abundance of 21-nt and 22-nt siRNAs with U residue at the 5′-terminus upon expression of HcPro and $8K^{P1}$ as compared to EP control and $8K^{P125}$.

In Arabidopsis, DCL2 is involved in processing viral and endogenous dsRNA into 22-nt siRNAs, especially when DCL4 is not active (Xie et al., 2004; Gasciolli et al., 2005; Bouche et al., 2006). Furthermore, DCL2 plays a crucial role in sense transgene-induced silencing and in transitivity (spread of a silencing state) of dsRNA-induced transgene silencing via expression of hairpin constructs (Mlotshwa et al., 2008; Parent et al., 2015). DCL2 also contributes to systemic spreading of transitive silencing between cells and through the vasculature (Taochy et al., 2017; Wu et al., 2017). Strikingly, our result from RT-qPCR show that accumulation of the antisense strand of 22-nt siRNAs is affected by expression of VSRs including $8K^{P1}$ and $8K^{P125}$.

It has been speculated that in addition to involvement in anti-viral and transgene RNA silencing, DCL2-dependent endogenous 22-nt sRNAs might affect endogenous gene expression and antivirus defence through secondary sRNA cascades (Wu et al., 2017; Taochy et al., 2017). Indeed, recently, it has been shown that DCL2 is the major Dicer in defence against potato virus X (PVX) and tobacco mosaic virus (TMV) in tomato (Wang et al., 2018). Tomato DCL2 is involved in the biogenesis of endogenous 22-nt sRNA including miR6026 that targets DCL2 mRNA and facilitates secondary sRNA production in a feed-back loop disrupted by the viruses (Wang et al., 2018). Interestingly, DCL2 expression levels increased in PVX- and TMV-infected tomato and the severity of viral symptoms was enhanced in the *dcl2ab* mutant (a double knock-out for *slDCL1a* and *slDCLb* genes) background, supporting the anti-viral role of DCL2 (Wang et al., 2018). It remains to be seen whether DCL2 has similar effects on PMTV and whether the DCL2-mediated sRNA pathway is manipulated by 8K for the benefit of the virus.

Accurate sorting of sRNAs into AGO-containing RISCs is paramount to proper functioning of RNA silencing pathways. In Arabidopsis, AGO1 and AGO2 play a primary role in anti-viral silencing (Brodersen et al., 2008). It was found that AGO1 preferentially binds to sRNAs with 5′-terminal U residue, whereas AGO2 prefers sRNAs with 5′-terminal A residue (Mi et al., 2008). Interestingly, through NGS analysis of siRNA we found lower amounts of siRNAs with U residue at the 5′-terminus upon expression of HC-Pro and $8K^{P1}$ as compared to EP control and $8K^{P125}$. Importantly, whereas there was a slight increase in the abundance sRNAs with A residue at the 5′-terminus in the HcPro and $8K^{P1}$ treatments, the increase was more pronounced for siRNAs with C residue at 5′-end upon expression of HcPro and $8K^{P1}$. Overall this data suggest that $8K^{P1}$ (and HcPro), but not $8K^{P125}$, might destabilise either sRNAs with U at 5′-terminus or complexes into which these sRNAs are sorted.

To conclude, our study demonstrates how positive selection could be shaping the activities of VSRs and emphasises importance of such studies for other viruses, because currently our knowledge on how variability of VSRs influence their activities is rather scarce. Our results uncovered several novel features of 8K functionality as a VSR as discussed above.

4. Materials and methods

4.1. Sequence alignment and phylogenetic analysis

Multiple alignment of PMTV 8K protein sequences was performed using MUSCLE in MEGA 7. Phylogenic analysis was performed using neighbour-joining method implemented in MEGA 7 (Kumar et al., 2016).

4.2. Construction of plasmids

For expression of constructs under the 35S promoter, PVA-HcPro, and 8K ORFs of isolates used in the study were amplified from plasmids carrying their respective full-length cDNA of PMTV RNA-TGB segment, using attB adapter flanked primers (Table S4). The PCR fragments were recombined into pDONR/Zeo vector using Gateway BP clonase II (Invitrogen). These entry clones were recombined into destination vector pGWB17 using Gateway LR clonase II (Invitrogen). For the mutagenesis of $8K^{P125}$, 8K gene was amplified using a forward primer carrying no mutation, and reverse primers carrying mutations at C18 and N50 sites, respectively (Table S4). The resulting product was cloned into RNA-TGB segment of P125 isolate using In-Fusion HD cloning kit (Clontech) following manufacturer's instructions. The mutant *C34AC36A* were obtained through PCR based site-directed mutagenesis of pDONR/Zeo-$8K^{Sw\_H}$ clone (Table S4) (Laible and Boonrod, 2009). The plasmids carrying these mutations were subsequently cloned into pGWB17 or pGWB15 as described above. All the constructs were verified by restriction digestion analysis, and sequencing.

4.3. Plant growth conditions

Nicotiana benthamiana plants were grown under long day conditions (16h light/8h dark) in a Phytotron growth chambers with minimum daytime temperature of 20 °C and night-time temperature of 18 °C.

4.4. Transient expression and inoculations

All plasmids were transformed in to *Agrobacterium tumefaciens* (strain C58C1), and were used for agroinfiltration at optical density at 600 nm (OD_{600}) of 0.5 into wild type *N. benthamina* leaves as described previously (Lukhovitskaya et al., 2013). One-day post infiltration, the leaves were rub-inoculated with in vitro generated transcripts of *XbaI* linearized TCV-sGFP plasmid, using T7 Ribomax large scale RNA production system (Promega) according to manufactures instructions. Prior to rub-inoculations, the transcripts were mixed with 3xGKP buffer [50 mM glycine, 30 mM K_2HPO_4 (pH 9.4), 1% (w/v) bentonite and 1% (w/v) celite]. In transient silencing suppression assay experiments, prior to agroinfiltration *Agrobacterium* carrying a reporter gene *GFP* and *Agrobacterium* carrying either, an empty vector, HcPro or 8K alleles were mixed in 1:1 ratio.

4.5. Fluorescence imaging and analysis

Four days post inoculation, the leaf samples were examined with Leica DMI 4000 inverted fluorescence microscope equipped with a DFC360 FX (CCD) camera. Images were taken with Lecia AF lite software. Mean area and intensity was measured using Fiji (ImageJ) software. Statistical analysis was performed using JMPpro software. GFP fluorescence in the detached whole leaves was detected using either a hand-held long-wave UV lamp UVL-56 (UV Products), or a Dual fluorescent protein flashlight (Nightsea, USA), and the pictures were taken with a Nikon D7200 camera. When Dual fluorescent protein flash light was used, images were taken using Canon EOS 7D camera, with the objective mounted with green-only bandpass filter (500–550 nm) to block blue and red reflected light.

4.6. Protein analysis

Forty-eight hours post agroinfiltrations, equal amounts of the leaf samples were homogenized in the 4x Laemmli extraction buffer (BioRad), boiled for 95 °C for 10min, centrifuged at 13,000 rpm for 10 min. Proteins were separated in 12% SDS-PAGE gels and transferred to nitrocellulose membrane. The nitrocellulose membrane was blocked with 5% (w/v) non-fat milk powder in tris-buffered saline containing 0.05% (v/v) Tween 20 (TBS-T). The expression of myc tagged proteins

and GFP proteins were assayed using mouse anti-myc-HRP, and anti-GFP-HRP monoclonal antibodies (Santa Cruz Biotechnology) at final dilutions of 1:1000 and 1:3000, respectively. A rat monoclonal anti-HA-peroxidase (Roche) was used to detect HA-tagged Sw H, and C34AC36A at a final dilution of 1:2000. The resulting chemiluminescent reaction was detected using the ECL Prime kit (Amersham, GE Healthcare) and LAS-3000 Luminescent Image Analyzer (Fujifilm, Fuji Photo Film).

4.7. RNA extraction and qPCR analysis

In order to quantify the GFP transcript level, total RNA was extracted using Spectrum Plant total RNA kit (Sigma-Aldrich) and On-column *DNase*I digestion Set (Sigma-Aldrich) according to the manufacturer's instructions. 1 μg of total RNA was used to perform reverse transcription using the iScript cDNA synthesis kit (Bio-Rad) according to the manufacturer's instructions. Four microliters of 10-fold diluted cDNA was used as a template for real-time PCR. Reactions were performed in a 20 μl reaction containing 2x DyNAmo Flash SYBR Green master mix (Thermo Scientific), ROX reference dye, and 0.3 μM primers specific for GFP. The GFP transcript level was normalized with a reference gene for Elongation Factor 1α (*EF-1α*). Quantifications were performed for three biological replicates, with three technical replicates for each biological replicate. Relative expression levels of GFP mRNA were calculated using ΔΔCT method (Livak, 1997).

4.8. siRNA sequencing and analysis

Total RNA was isolated using the mirVana miRNA isolation kit (Ambion) according to the manufacturer's instructions and the RNA quality was tested with the aid of Agilent Bioanalyzer chips. The sequencing was performed with an Illumina HiSeq2500 sequencing platform with High Output mode, SR 1x50bp at SciLife sequencing facility, Stockholm. Raw reads quality assessment was performed using FastQC (version 0.11.3). Quality control of raw reads was performed through cutadapt (version 1.2.1) with minimal sequence length after adaptor removal 18 (Martin, 2011). The clean reads for each sample was aligned to the reference sequence using Bowtie v1.2.2 with two mismatches allowed per seed (-N 2), a seed length of 18 (-L 18), no mismatch in read alignment (v 0) and the rest of alignment parameters set to their default values. SAM alignment files produced by Bowtie were converted to BAM files, sorted, and indexed using SAMtools v0.1.19 (Li and Durbin, 2009)(Li and Durbin, 2009). The number reads per samples, sense/antisense, locations, lengths, coverage and orientations of reads mapping to the references were obtained through SAMtools and custom bash scripts. Read count for each samples and length were normalized into reads per million (RPM).

4.9. siRNA and miRNA quantification

Stem-loop reverse transcription (RT) primers were synthesized as described previously (Varkonyi-Gasic and Hellens, 2011). Stem-loop RT was carried out with the same RNA template that was used for the NGS analysis. Briefly, 12.5 μl RNA and water, together with 0.5 μl of 10 mM dNTP (Thermo Scientific) was incubated at 65 °C for 5 min, and immediately transferred to ice. A mixture containing 4 μl of 5x SSIV buffer, 2 μl of 0.1M DTT, 0.1 μl of RiboLock RNase inhibitor (40U/μl), and 0.25 μl of SSIV reverse transcriptase (Thermo Scientific), and 1 μl of 10 mM respective stem-loop RT primer was added to the RNA. Thereafter, the tubes were incubated in a thermal cycler with the following conditions, 16 °C for 30 min, 42 °C for 30 min, 85 °C for 5 min, and held at 4 °C. All stem-loop RT reactions included no RNA template controls, and RT minus controls. Additionally, RT reaction was carried out for *PP2A* gene using gene-specific reverse primer with each of the samples, with the above conditions.

Real-time PCR was performed using standard DyNAmo Flash SYBR Green kit protocol (Thermo Scientific). The 20 μl PCR included 2x DyNAmo Flash SYBR Green master mix (Thermo Scientific), ROX reference dye, and 0.3 μM forward primer targeting specific siRNA or miRNA, and 0.3 μM of universal reverse primer. The Ct values of siRNA or miRNA expression was normalized to the Ct values of *PP2A* gene. The Relative fold expression was quantified using ΔΔCT method (Livak, 1997).

Acknowledgements

We thank Tim L. Sit and Steven A. Lommel (Dept. of Plant Pathology, North Carolina State University) for the TCV-sGFP construct. This work was supported by the Swedish Research Council Formas (Grants 2014-01018, 2018-00591 to EIS; Grant 2015-00430 to LGB), the Swedish Foundation for Strategic Research (SSF), through a Future Research Leaders Grant (FFL5) to LGB, and Helge Axelsson Johnssons foundation. Sequencing was performed by the Science for Life Laboratory Platform in Stockholm. We acknowledge support from Science for Life Laboratory, the Knut and Alice Wallenberg Foundation, the National Genomics Infrastructure funded by the Swedish Research Council, and Uppsala Multidisciplinary Center for Advanced Computational Science for assistance with massively parallel sequencing (alternatively genotyping) and access to the UPPMAX computational infrastructure. We declare that we have no conflict of interests.

Appendix A. Supplementary data

Supplementary data to this article can be found online at https://doi.org/10.1016/j.virol.2019.06.018.

References

Adams, M.J., Antoniw, J.F., Kreuze, J., 2009. Virgaviridae: a new family of rod-shaped plant viruses. Arch. Virol. 154, 1967–1972.
Baksa, I., Nagy, T., Barta, E., Havelda, Z., Varallyay, E., Silhavy, D., Burgyan, J., Szittya, G., 2015. Identification of Nicotiana benthamiana microRNAs and their targets using high throughput sequencing and degradome analysis. BMC Genomics 16, 1025.
Bouche, N., Lauressergues, D., Gasciolli, V., Vaucheret, H., 2006. An antagonistic function for Arabidopsis DCL2 in development and a new function for DCL4 in generating viral siRNAs. EMBO J. 25, 3347–3356.
Brodersen, P., Sakvarelidze-Achard, L., Bruun-Rasmussen, M., Dunoyer, P., Yamamoto, Y.Y., Sieburth, L., Voinnet, O., 2008. Widespread translational inhibition by plant miRNAs and siRNAs. Science 320, 1185–1190.
Calvert, E.L., Harrison, B.D., 1966. Potato mop-top, a soil-borne virus. Plant Pathol. 15, 134–139.
Chen, H.Y., Yang, J., Lin, C., Yuan, Y.A., 2008. Structural basis for RNA-silencing suppression by Tomato aspermy virus protein 2b. EMBO Rep. 9, 754–760.
Coffey, L.L., Beeharry, Y., Bordería, A.V., Blanc, H., Vignuzzi, M., 2011. Arbovirus high fidelity variant loses fitness in mosquitoes and mice. Proc. Natl. Acad. Sci. U.S.A. 108 (38), 16038–16043. https://doi.org/10.1073/pnas.1111650108.
Csorba, T., Kontra, L., Burgyan, J., 2015. Viral silencing suppressors: tools forged to fine-tune host-pathogen coexistence. Virology 479–480, 85–103.
Deleris, A., Gallego-Bartolome, J., Bao, J., Kasschau, K.D., Carrington, J.C., Voinnet, O., 2006. Hierarchical action and inhibition of plant Dicer-like proteins in antiviral defense. Science 313, 68–71.
Fagard, M., Boutet, S., Morel, J.B., Bellini, C., Vaucheret, H., 2000. AGO1, QDE-2, and RDE-1 are related proteins required for post-transcriptional gene silencing in plants, quelling in fungi, and RNA interference in animals. Proc. Natl. Acad. Sci. U. S. A. 97, 11650–11654.
Fukudome, A., Kanaya, A., Egami, M., Nakazawa, Y., Hiraguri, A., Moriyama, H., Fukuhara, T., 2011. Specific requirement of DRB4, a dsRNA-binding protein, for the in vitro dsRNA-cleaving activity of Arabidopsis Dicer-like 4. RNA 17, 750–760.
Garcia-Ruiz, H., Carbonell, A., Hoyer, J.S., Fahlgren, N., Gilbert, K.B., Takeda, A., Giampetruzzi, A., Garcia Ruiz, M.T., Mcginn, M.G., Lowery, N., Martinez Baladejo, M.T., Carrington, J.C., 2015. Roles and programming of Arabidopsis ARGONAUTE proteins during Turnip mosaic virus infection. PLoS Pathog. 11, e1004755.
Gasciolli, V., Mallory, A.C., Bartel, D.P., Vaucheret, H., 2005. Partially redundant functions of Arabidopsis DICER-like enzymes and a role for DCL4 in producing trans-acting siRNAs. Curr. Biol. 15, 1494–1500.
Gil, J.F., Adams, I., Boonham, N., Nielsen, S.L., Nicolaisen, M., 2016. Molecular and biological characterisation of two novel pomo-like viruses associated with potato (Solanum tuberosum) fields in Colombia. Arch. Virol. 161, 1601–1610.
Gonzalez-Jara, P., Atencio, F.A., Martinez-Garcia, B., Barajas, D., Tenllado, F., Diaz-Ruiz, J.R., 2005. A single amino acid mutation in the plum pox virus helper component-proteinase gene abolishes both synergistic and RNA silencing suppression activities. Phytopathology 95, 894–901.
Haas, G., Azevedo, J., Moissiard, G., Geldreich, A., Himber, C., Bureau, M., Fukuhara, T.,

Keller, M., Voinnet, O., 2008. Nuclear import of CaMV P6 is required for infection and suppression of the RNA silencing factor DRB4. EMBO J. 27, 2102–2112.
Hamilton, A.J., Baulcombe, D.C., 1999. A species of small antisense RNA in post-transcriptional gene silencing in plants. Science 286, 950–952.
Hiraguri, A., Itoh, R., Kondo, N., Nomura, Y., Aizawa, D., Murai, Y., Koiwa, H., Seki, M., Shinozaki, K., Fukuhara, T., 2005. Specific interactions between Dicer-like proteins and HYL1/DRB-family dsRNA-binding proteins in Arabidopsis thaliana. Plant Mol. Biol. 57, 173–188.
Iki, T., Tschopp, M.A., Voinnet, O., 2017. Biochemical and genetic functional dissection of the P38 viral suppressor of RNA silencing. RNA 23, 639–654.
International Potato Center, 2017. Annual report 2017 [Online]. Available: https://cipotato.org/annualreport2017/, Accessed date: 30 September 2018.
Jin, H., Zhu, J.K., 2010. A viral suppressor protein inhibits host RNA silencing by hooking up with Argonautes. Genes Dev. 24, 853–856.
Kalyandurg, P., Gil, J.F., Lukhovitskaya, N.I., Flores, B., Muller, G., Chuquillanqui, C., Palomino, L., Monjane, A., Barker, I., Kreuze, J., Savenkov, E.I., 2017. Molecular and pathobiological characterization of 61 Potato mop-top virus full-length cDNAs reveals great variability of the virus in the centre of potato domestication, novel genotypes and evidence for recombination. Mol. Plant Pathol. 18, 864–877.
Kashiwazaki, S., Scott, K.P., Reavy, B., Harrison, B.D., 1995. Sequence analysis and gene content of potato mop-top virus RNA 3: further evidence of heterogeneity in the genome organization of furoviruses. Virology 206, 701–706.
Kumar, S., Stecher, G., Tamura, K., 2016. MEGA7: molecular evolutionary genetics analysis version 7.0 for bigger datasets. Mol. Biol. Evol. 33, 1870–1874.
Lacombe, S., Bangratz, M., Vignols, F., Brugidou, C., 2010. The rice yellow mottle virus P1 protein exhibits dual functions to suppress and activate gene silencing. Plant J. 61, 371–382.
Laible, M., Boonrod, K., 2009. Homemade site directed mutagenesis of whole plasmids. J. Vis. Exp. (27), e1135. https://doi.org/10.3791/1135.
Laird, J., Mcinally, C., Carr, C., Doddiah, S., Yates, G., Chrysanthou, E., Khattab, A., Love, A.J., Geri, C., Sadanandom, A., Smith, B.O., Kobayashi, K., Milner, J.J., 2013. Identification of the domains of cauliflower mosaic virus protein P6 responsible for suppression of RNA silencing and salicylic acid signalling. J. Gen. Virol. 94, 2777–2789.
Li, H., Durbin, R., 2009. Fast and accurate short read alignment with Burrows-Wheeler transform. Bioinformatics 25, 1754–1760.
Li, F., Huang, C., Li, Z., Zhou, X., 2014. Suppression of RNA silencing by a plant DNA virus satellite requires a host calmodulin-like protein to repress RDR6 expression. PLoS Pathog. 10, e1003921.
Livak, K.J., 1997. Relative Quantitation of Gene Expression. PE Applied Biosystems, Foster City, CA, pp. 11–15.
Lukhovitskaya, N.I., Yelina, N.E., Zamyatnin Jr., A.A., Schepetilnikov, M.V., Solovyev, A.G., Sandgren, M., Morozov, S.Y., Valkonen, J.P., Savenkov, E.I., 2005. Expression, localization and effects on virulence of the cysteine-rich 8 kDa protein of Potato mop-top virus. J. Gen. Virol. 86, 2879–2889.
Lukhovitskaya, N.I., Thaduri, S., Garushyants, S.K., Torrance, L., Savenkov, E.I., 2013. Deciphering the mechanism of defective interfering RNA (DI RNA) biogenesis reveals that a viral protein and the DI RNA act antagonistically in virus infection. J. Virol. 87, 6091–6103.
Margis, R., Fusaro, A.F., Smith, N.A., Curtin, S.J., Watson, J.M., Finnegan, E.J., Waterhouse, P.M., 2006. The evolution and diversification of Dicers in plants. FEBS Lett. 580, 2442–2450.
Martin, M., 2011. Cutadapt removes adapter sequences from high-throughput sequencing reads. EMBnet J. 17, 10–12.
Mi, S.J., Cai, T., Hu, Y.G., Chen, Y., Hodges, E., Ni, F.R., Wu, L., Li, S., Zhou, H., Long, C.Z., Chen, S., Hannon, G.J., Qi, Y.J., 2008. Sorting of small RNAs into Arabidopsis argonaute complexes is directed by the 5 ' terminal nucleotide. Cell 133, 116–127.
Mlotshwa, S., Pruss, G.J., Peragine, A., Endres, M.W., Li, J., Chen, X., Poethig, R.S., Bowman, L.H., Vance, V., 2008. DICER-LIKE2 plays a primary role in transitive silencing of transgenes in Arabidopsis. PLoS One 3, e1755.
Molnar, A., Melnyk, C.W., Bassett, A., Hardcastle, T.J., Dunn, R., Baulcombe, D.C., 2010. Small silencing RNAs in plants are mobile and direct epigenetic modification in recipient cells. Science 328, 872–875.
Murray, G.G., Kosakovsky Pond, S.L., Obbard, D.J., 2013. Suppressors of RNAi from plant viruses are subject to episodic positive selection. Proc. Biol. Sci. 280, 20130965.
Nakagawa, T., Kurose, T., Hino, T., Tanaka, K., Kawamukai, M., Niwa, Y., Toyooka, K., Matsuoka, K., Jinbo, T., Kimura, T., 2007. Development of series of gateway binary vectors, pGWBs, for realizing efficient construction of fusion genes for plant transformation. J. Biosci. Bioeng. 104, 34–41.
Nemes, K., Gellert, A., Almasi, A., Vagi, P., Saray, R., Kadar, K., Salanki, K., 2017. Phosphorylation regulates the subcellular localization of Cucumber Mosaic Virus 2b protein. Sci. Rep. 7.
Odokonyero, D., Mendoza, M.R., Moffett, P., Scholthof, H.B., 2017. Tobacco rattle virus (TRV)-mediated silencing of *Nicotiana benthamiana* Argonautes (NbAGOs) reveals new antiviral candidates and dominant effects of TRV-NbAGO1. Phytopathology 107, 977–987.
Okano, Y., Senshu, H., Hashimoto, M., Neriya, Y., Netsu, O., Minato, N., Yoshida, T., Maejima, K., Oshima, K., Komatsu, K., Yamaji, Y., Namba, S., 2014. In Planta Recognition of a double-stranded RNA synthesis protein complex by a Potexviral RNA silencing suppressor. Plant Cell 26, 2168–2183.
Parent, J.S., Bouteiller, N., Elmayan, T., Vaucheret, H., 2015. Respective contributions of Arabidopsis DCL2 and DCL4 to RNA silencing. Plant J. 81, 223–232.
Pfeiffer, J.K., Kirkegaard, K., 2005. Increased fidelity reduces poliovirus fitness and virulence under selective pressure in mice. PLoS Pathog. 1, e11. https://doi.org/10.1371/journal.ppat.0010011.
Powers, J.G., Sit, T.L., Qu, F., Morris, T.J., Kim, K.H., Lommel, S.A., 2008. A versatile assay for the identification of RNA silencing suppressors based on complementation of viral movement. Mol. Plant Microbe Interact. 21, 879–890.
Qu, F., Ren, T., Morris, T.J., 2003. The coat protein of Turnip crinkle virus suppresses posttranscriptional gene silencing at an early initiation step. J. Virol. 77, 511–522.
Qu, F., Ye, X., Morris, T.J., 2008. Arabidopsis DRB4, AGO1, AGO7, and RDR6 participate in a DCL4-initiated antiviral RNA silencing pathway negatively regulated by DCL1. Proc. Natl. Acad. Sci. U. S. A. 105, 14732–14737.
Reavy, B., Arif, M., Cowan, G.H., TorranCE, L., 1998. Association of sequences in the coat protein/readthrough domain of potato mop-top virus with transmission by Spongospora subterranea. J. Gen. Virol. 79, 2343–2347.
Sahana, N., Kaur, H., Jain, R.K., Palukaitis, P., Canto, T., Praveen, S., 2014. The asparagine residue in the FRNK box of potyviral helper-component protease is critical for its small RNA binding and subcellular localization. J. Gen. Virol. 95, 1167–1177.
Savenkov, E.I., Sandgren, M., Valkonen, J.P., 1999. Complete Sequence of RNA 1 and the presence of tRNA-like structures in all RNAs of Potato mop-top virus, genus Pomovirus. J. Gen. Virol. 2779–2784.
Scott, K.P., Kashiwazaki, S., Reavy, B., Harrison, B.D., 1994. The nucleotide sequence of potato mop-top virus RNA 2: a novel type of genome organization for a furovirus. J. Gen. Virol. 75, 3561–3568.
Sereme, D., Lacombe, S., Konate, M., Bangratz, M., Pinel-Galzi, A., Fargette, D., Traore, A.S., Konate, G., Brugidou, C., 2014. Sites under positive selection modulate the RNA silencing suppressor activity of rice yellow mottle virus movement protein P1. J. Gen. Virol. 95, 213–218.
Silhavy, D., Molnar, A., Lucioli, A., Szittya, G., Hornyik, C., Tavazza, M., Burgyan, J., 2002. A viral protein suppresses RNA silencing and binds silencing-generated, 21- to 25-nucleotide double-stranded RNAs. EMBO J. 21, 3070–3080.
Sire, C., Bangratz-Reyser, M., Fargette, D., Brugidou, C., 2008. Genetic diversity and silencing suppression effects of Rice yellow mottle virus and the P1 protein. Virol. J. 5.
Taochy, C., Gursanscky, N.R., Cao, J., Fletcher, S.J., Dressel, U., Mitter, N., Tucker, M.R., Koltunow, A.M.G., Bowman, J.L., Vaucheret, H., Carroll, B.J., 2017. A genetic screen for impaired systemic RNAi highlights the crucial role of DICER-LIKE 2. Plant Physiol. 175, 1424–1437.
Torres-Barcelo, C., Martin, S., Daros, J.A., Elena, S.F., 2008. From hypo- to hypersuppression: effect of amino acid substitutions on the RNA-silencing suppressor activity of the Tobacco etch potyvirus HC-Pro. Genetics 180, 1039–1049.
Torres-Barcelo, C., Daros, J.A., Elena, S.F., 2010. Compensatory molecular evolution of HC-Pro, an RNA-silencing suppressor from a plant RNA virus. Mol. Biol. Evol. 27, 543–551.
Valli, A.A., Gallo, A., Rodamilans, B., Lopez-Moya, J.J., Garcia, J.A., 2018. The HCPro from the Potyviridae family: an enviable multitasking Helper Component that every virus would like to have. Mol. Plant Pathol. 19, 744–763.
Varallyay, E., Havelda, Z., 2013. Unrelated viral suppressors of RNA silencing mediate the control of ARGONAUTE1 level. Mol. Plant Pathol. 14, 567–575.
Varkonyi-Gasic, E., Hellens, R.P., 2011. Quantitative stem-loop RT-PCR for detection of microRNAs. Methods Mol. Biol. 744, 145–157.
Wang, X.B., Jovel, J., Udomporn, P., Wang, Y., Wu, Q., Li, W.X., Gasciolli, V., Vaucheret, H., Ding, S.W., 2011. The 21-nucleotide, but not 22-nucleotide, viral secondary small interfering RNAs direct potent antiviral defense by two cooperative argonautes in Arabidopsis thaliana. Plant Cell 23, 1625–1638.
Wang, Z., Hardcastle, T.J., Canto Pastor, A., Yip, W.H., Tang, S., Baulcombe, D.C., 2018. A novel DCL2-dependent miRNA pathway in tomato affects susceptibility to RNA viruses. Genes Dev. 32, 1155–1160. https://doi.org/10.1101/gad.313601.118.
Wu, Y.Y., Hou, B.H., Lee, W.C., Lu, S.H., Yang, C.J., Vaucheret, H., Chen, H.M., 2017. DCL2- and RDR6-dependent transitive silencing of SMXL4 and SMXL5 in Arabidopsis dcl4 mutants causes defective phloem transport and carbohydrate over-accumulation. Plant J. 90, 1064–1078.
Xie, Z., Johansen, L.K., Gustafson, A.M., Kasschau, K.D., Lellis, A.D., Zilberman, D., Jacobsen, S.E., Carrington, J.C., 2004. Genetic and functional diversification of small RNA pathways in plants. PLoS Biol. 2, E104.
Yambao, M.L., Yagihashi, H., Sekiguchi, H., Sekiguchi, T., Sasaki, T., Sato, M., Atsumi, G., Tacahashi, Y., Nakahara, K.S., Uyeda, I., 2008. Point mutations in helper component protease of clover yellow vein virus are associated with the attenuation of RNA-silencing suppression activity and symptom expression in broad bean. Arch. Virol. 153, 105–115.
Zhang, X., Du, P., Lu, L., Xiao, Q., Wang, W., Cao, X., Ren, B., Wei, C., Li, Y., 2008. Contrasting effects of HC-Pro and 2b viral suppressors from Sugarcane mosaic virus and Tomato aspermy cucumovirus on the accumulation of siRNAs. Virology 374, 351–360.
Zhang, X., Zhang, X., Singh, J., Li, D., Qu, F., 2012. Temperature-dependent survival of Turnip crinkle virus-infected arabidopsis plants relies on an RNA silencing-based defense that requires dcl2, AGO2, and HEN1. J. Virol. 86, 6847–6854.
Zhang, X., Dong, K., Xu, K., Zhang, K., Jin, X.J., Yang, M., Zhang, Y.L., Wang, X.B., Han, C.G., Yu, J.L., Li, D.W., 2018. Barley stripe mosaic virus infection requires PKA-mediated phosphorylation of gamma b for suppression of both RNA silencing and the host cell death response. New Phytol. 218, 1570–1585.